Polyethersulfone/poly(acrylic acid) composite hydrogel membrane reservoirs for controlled delivery of cationic drug formulations

Željko Janićijević [a,b], Filip Radovanović [b,*]

[a]*University of Belgrade, School of Electrical Engineering, Bulevar kralja Aleksandra 73, 11120 Belgrade, Serbia*

[b]*Institute of Technical Sciences of the Serbian Academy of Sciences and Arts, Knez Mihailova 35/IV, 11000 Belgrade, Serbia*

**Corresponding author:* Dr. Filip Radovanović

Institute of Technical Sciences of the Serbian Academy of Sciences and Arts, Knez Mihailova 35/IV,11000 Belgrade, Serbia

E-mail address: filip.radovanovic@itn.sanu.ac.rs

Abstract

We present the innovative synthesis of polyethersulfone/poly(acrylic acid) composite hydrogel membranes performed by combining photoirradiation with a traditional liquid phase inversion process. Fabricated membranes exhibited ion exchange capacity and water content as high as 5.2 mmol/g and 75%, respectively. The chemical composition of the membranes was determined using FTIR-ATR and their microstructure was examined with SEM. Our findings suggest that the use of hydrophilic crosslinker was crucial for the synthesis of symmetric and mechanically stable composite hydrogel membranes. Passive and iontophoretic release kinetics from membrane reservoirs synthesized with the hydrophilic crosslinker were investigated *in vitro* using methylene blue as a model drug. Passive release kinetics was diffusion-controlled with pH-sensitive and loading-dependent behavior. Linear release kinetics was demonstrated during the iontophoretic release.

Synthesized composite hydrogel membranes hold a lot of promise as compact stand-alone reservoirs for passive and iontophoretic delivery of cationic drugs.

Keywords: composite hydrogel membrane; crosslinker; ion exchange; diffusion; iontophoresis; drug release

1. Introduction

Hydrogels are polymeric networks with three-dimensional structure and capability to absorb large amounts of water or biological fluids [1]. Their unique properties, such as high water content, porosity, and soft consistency, closely resemble those of biological tissues, and therefore hydrogels represent an important class of synthetic biomaterials [2]. In controlled drug delivery applications, the main advantage of hydrogels is the possibility to provide prolonged sustained release of the active ingredient [3,4]. Hydrogels can also respond to different internal or external stimuli, by changing their structure, swelling behavior, permeability or mechanical properties, which may be used to modulate drug release [5]. Moreover, hydrogels have been used as drug reservoirs for transdermal iontophoretic delivery of drugs [6].

Poly(acrylic acid) (PAA) hydrogel is an interesting material for the storage of cationic drug formulations. Presence of carboxyl groups in this hydrogel enables cation exchange [7], while their volume distribution imparts electrical conductivity [8]. Hence, PAA has the potential to be applied as a versatile drug matrix for passive delivery via ion exchange or active delivery via iontophoresis.

Active delivery via iontophoresis implies the application of small physiologically acceptable electric current for driving the charged and neutral drugs into the body [9,10]. Ion exchange fibers were successfully used as drug reservoirs in iontophoresis by Jaskari and coworkers [11]. The same research group also demonstrated efficient use of ion exchange fibers for iontophoretic transdermal delivery of apomorphine [12] and leuprorelin [13]. Using tramadol as a model drug, Gao and coworkers showed that ion exchange fibers exhibited uniform drug loading and controllable iontophoretic delivery [14]. In a study by Vispute et al. it was concluded that ion exchange fibers have superior iontophoretic properties in terms of cationic drug loading and release compared to ion exchange resins [15]. Although ion exchange fibers have a high binding capacity for charged drugs and

adequate properties for iontophoresis, their drug release properties cannot be easily customized for specific applications. In addition, they need to be packed and enclosed to form a usable drug reservoir with defined geometry.

Composite hydrogel membranes combining soft functional hydrogel and a rigid porous membrane are a class of materials that can be of interest in various applications, such as sensing and analytics, biomedical engineering, as well as the controlled drug delivery [16]. These membranes can commonly be tailored with a specific purpose in mind and directly fabricated in the desired form with well-defined shape and thickness. Therefore, composite hydrogel membranes are good candidates for compact drug reservoirs which do not require dedicated packaging. Relevant properties of such composite drug reservoirs could be adjusted for a specific application already during membrane synthesis and without subsequent fabrication steps required to form the reservoir.

Composite hydrogel membranes containing PAA were investigated in the past for various applications. pH-sensitive valves were synthesized by *in situ* polymerization and crosslinking of acrylic acid (AA) within the pores of poly(vinylidene fluoride) (PVDF) membrane [17]. Blending of polyethersulfone (PES) solution with (PAA) microgels was used to synthesize composite membranes with pH sensitivity and potential for ion exchange applications [18]. Ion exchange ultrafiltration membranes were obtained by mixing polysulfone and PAA solutions followed by liquid phase inversion of the cast films [19]. *In situ* crosslinked copolymerization of N-vinylpyrrolidone and AA in PES solutions was used to synthesize multifunctional composite membranes. After copolymerization at elevated temperature, spin coating, and liquid-liquid phase inversion were applied to form the membranes which exhibited good biocompatibility and ability to adsorb cationic dyes [20]. Composite hydrogel membranes synthesized by combining photopolymerization and liquid phase inversion were investigated for proton conducting applications [21] and removal of heavy metals [22].

In this work, we present the synthesis and characterization of composite hydrogel membrane reservoirs intended for controlled delivery of cationic drug formulations. Our composite membrane design comprises a PES polymeric base and a crosslinked PAA hydrogel with pH-responsive carboxyl groups. We specifically evaluated the influence of different crosslinkers on basic membrane properties. Membranes were fabricated by sequential

application of photoirradiation and immersion precipitation of the cast film containing all functional components. Scanning electron microscopy (SEM) and Fourier transform infrared spectroscopy-Attenuated total reflection (FTIR-ATR) were used to examine composite membrane morphology and spatial distribution of resulting phases. We also investigated loading and *in vitro* release kinetics of methylene blue (MB), and demonstrated the potential of these membranes as reservoirs for iontophoretic delivery. MB dye was selected as the model drug due to the promising results obtained in the management of chronic wounds, such as pressure injuries and diabetic ulcers, with antibacterial dressings containing MB [23,24].

The composite hydrogel membranes described in this work can potentially be used as multipurpose stand-alone drug reservoirs with specifically tailored properties in the applications requiring passive or iontophoretic transdermal drug delivery. Most membrane properties of interest for drug loading and delivery can be simply adjusted by modifying the composition of the casting solution.

2. Experimental

2.1 Materials

PES (Ultrason E 6020P, M_w = 75,000, PDI 3.4) was kindly provided by BASF (Badische Anilin- und Soda-Fabrik), Germany. Polyester spunbond nonwoven fabric (Type 078/20) of area weight 21 g/m^2 was kindly supplied by Johns Manville Sales GmbH, Germany. N-methyl-2-pyrrolidone (NMP) (99% purity), AA, *N*, *N*′-Methylenebis(acrylamide) (MBAA) and trimethylolpropane ethoxylate triacrylate (TMPTA) (average M_n = 912) were obtained from Sigma-Aldrich, Germany. Photoinitiator (PI), bis(2,4,6-trimethylbenzoyl)-phenylphosphineoxide (Irgacure 819), was kindly provided by Ciba SC, Switzerland. MB powder was purchased from E. Merck, Germany. Potassium dihydrogen phosphate (KH_2PO_4) (p. a.) and sodium hydroxide (NaOH) (p. a.) were supplied by Centrohem, Serbia. Citric acid monohydrate was obtained from Alkaloid, Former Yugoslav Republic of Macedonia. Ethanol (96% vol.) was purchased from Zorka Pharma, Serbia. Hydrochloric acid (HCl) (37%) was supplied by BDH Prolabo, France. All chemicals were used as received without further purification.

Tap water was used in the coagulation bath for all membrane synthesis experiments. Distilled water was used to prepare solutions for experimental analysis of membrane ion exchange capacity, membrane swelling degree, MB absorption, MB release kinetics and iontophoretic transport of MB.

2.2 Membrane synthesis

For the synthesis of composite PES membranes, the traditional liquid phase inversion process was modified by incorporating AA and a bifunctional (MBAA) or trifunctional (TMPTA) crosslinker in the polymer casting solution and copolymerizing them before the immersion in water and final solidification step. A 30% by weight solution of PES in NMP was prepared by mixing at 80 °C overnight. Solutions of AA, MBAA or TMPTA, and PI in NMP were freshly prepared by mixing the components in amber vials cooled with ice and protected from ambient light. Each solution for making membranes was prepared by mixing a given quantity of PES with a solution of photopolymerizable components just prior to the casting. All prepared solutions were transparent confirming complete miscibility of the components. PES concentration in solutions prepared for casting is expressed in percentage by weight. AA concentration is expressed in mmols per g of the final dry membrane at a theoretical 100% reactant conversion. The concentration of the crosslinking agent is expressed as a mole percentage based on the AA concentration.

Prepared solutions were cast on a glass plate using a 7.62 cm-wide film applicator with a 200 μm gap (BYK Gardner), then put in an experimental enclosure blanketed with nitrogen gas and exposed to UV irradiation through a glass window on top of the enclosure for 3 min. The exposure dose, mainly in the UVA region, was 1.5 J/cm^2, as measured by the YK-35UV light meter, Taiwan. UV exposure initiated polymerization and crosslinking of AA to create a gel in the cast film. After UV curing, cast films were immersed in the water bath to form membranes. After allowing at least 10 min to complete phase separation and solidification, membranes were further extracted in distilled water overnight in order to remove residual solvent, unreacted monomers, and PI. Membranes were then stored in an ethanol/water 1:1 (v/v) mixture to prevent microbial contamination.

2.3 Membrane characterization

FTIR-ATR analysis was conducted with Thermo Scientific Nicolet 6700 instrument equipped with Smart ATR Diamond accessory, USA. The spectra were recorded in the range of 525-4000 cm^{-1} with the resolution of 0.5 cm^{-1} and then normalized to the highest peak intensity.

Microstructural properties were examined by recording the fracture surfaces of membrane specimens with the field emission SEM (TESCAN MIRA 3 XMU, Czech Republic). Wet membrane samples were dipped for 1 h in ethanol, then 1 h in heptane to minimize pore collapse during sample preparation, followed by air drying for at least 24 h at ambient temperature. Prior to the recording, dry membrane samples were cooled in liquid nitrogen, fractured and sputtered with carbon.

2.3.1 Mass swelling degree (SD) and water content (WC)

Prior to the experiments, membranes were equilibrated in distilled water, phosphate buffer solution (pH = 8 and I = 0.2 M), and citrate buffer solution (pH = 3 and I = 0.2 M) or immersed into MB absorption solutions for 24 h in the dark.

At the beginning of each experiment, a wet membrane specimen of the approximate area of 1 cm^2 was cut out from the membrane sheet and its mass was measured. The specimen was subsequently dried in an oven at 100 °C for 2 h, and finally, the mass of the dry membrane specimen was determined. All experiments were performed in triplicate.

SD was calculated based on the wet membrane mass at time *t*, m_t, and the dry membrane mass, m_0, measured at the end of the experiment, according to the following formula:

$$SD = \frac{(m_t - m_0)}{m_0} \cdot 100\ (\%) \tag{1}$$

WC of the membrane specimen was calculated using the following equation:

$$WC = \frac{100 \cdot SD}{(100 + SD)}\ (\%) \tag{2}$$

2.3.2 Determination of carboxyl group concentration (C_{cg})

Determination of C_{cg} was carried out using the potentiometric acid-base titration method. A small membrane sample (30-50 mg of dry mass) was cut into pieces and immersed in 10 ml of 1 M HCl solution. The solution was stirred for 1 h to protonate all carboxyl groups in the sample and then the sample was thoroughly rinsed with distilled water. The protonated membrane sample was subsequently submerged in 40 ml of 0.01 M NaOH solution and the mixture was stirred again for 1h in a capped beaker. The membrane sample was then separated from the residual solution, rinsed with distilled water, dried for 2 h at 100 °C, and the dry mass of the membrane sample was finally weighed. Aliquots of 15 ml of residual solution were titrated with 0.01 M HCl and change in pH was monitored with a pH-meter (HI 3222, Hanna Instruments, Romania) to determine the equivalence point. As a blank probe, 15 ml of 0.01 M NaOH solution was titrated with 0.01 M HCl. All experiments were performed in duplicate.

C_{cg} was calculated according to the following expression:

$$C_{cg}(\mathrm{mmol/g}) = 0.4(1 - V_2/V_1)/W_d \quad (3)$$

where V_1 is the volume of 0.01 M HCl solution consumed for the titration of the blank probe, V_2 is the volume of 0.01 M HCl solution consumed for the titration of the residual solution aliquot, and W_d is the mass of dry membrane sample.

2.3.3 Absorption of MB

A wet membrane sample of the approximate area of 1 cm^2 was cut out from the membrane sheet and equilibrated in 50 ml of phosphate buffer solution (pH = 8 and I = 0.2 M). The membrane sample was then rinsed with distilled water and its wet mass was measured. Finally, the wet membrane sample was immersed in 50 ml of aqueous solution of MB for 24 h at room temperature. The concentration of MB in prepared solutions was adjusted to target molar ratios of MB cations and carboxyl groups in the membrane sample at a theoretical 100% conversion, $n(MB^+)/n(\text{-COOH})$, of 0.5, 1, or 1.5, which is similar to the experimental conditions used by Gao et al. [14] to study the loading efficiency of ion-exchange fibers. The initial concentration of MB in the

solution was calculated using the wet membrane mass, mean SD and mean concentration of the carboxyl groups. Experiments were replicated three times for each condition.

2.3.4 Release of MB

Membrane sample containing the absorbed dye was rinsed with distilled water and its surface was carefully blotted with a paper tissue. Prepared sample was subsequently immersed in 200 ml of phosphate buffer solution (pH = 8 and I = 0.2 M) or citrate buffer solution (pH = 3 and I = 0.2 M). The solution was then stirred at 500 rpm at ambient temperature. Solution aliquots of 3 ml were taken at predefined time intervals to follow the release kinetics and immediately replaced with the same volume of fresh buffer. Release kinetics was monitored with the UV-Vis spectrophotometer (GBC Cintra 101, Australia) at the absorption wavelength of 664 nm. After coming close to the saturation point, the solution was left to equilibrate with the sample for at least 48 h at ambient temperature in the dark. The total released amount of MB in equilibrium was then measured.
After the desorption experiment, membrane sample was again rinsed with distilled water and its surface was carefully blotted with a tissue paper. The sample was transferred to a beaker, soaked in 50 ml of 96% (vol.) ethanol and stirred at 1100 rpm at room temperature for 3 h. Released amount of MB in the solution was then determined with the UV-Vis spectrophotometer. At the end of the release experiments, membrane sample was dried for 1 h at 100 °C and its dry mass was measured. Release experiments were performed in duplicate for each set of experimental conditions.

2.3.5 In vitro iontophoresis experiment

Iontophoresis experiment was performed in a custom built side-by-side cell made of acrylic glass with the circular cross-section of 1 cm in diameter illustrated in **Fig. 1**. Junctions were sealed with silicon grease or thread seal tape to prevent leakage of the solutions throughout the experiment. The experiment was conducted in two steps: MB absorption and iontophoretic release of MB.

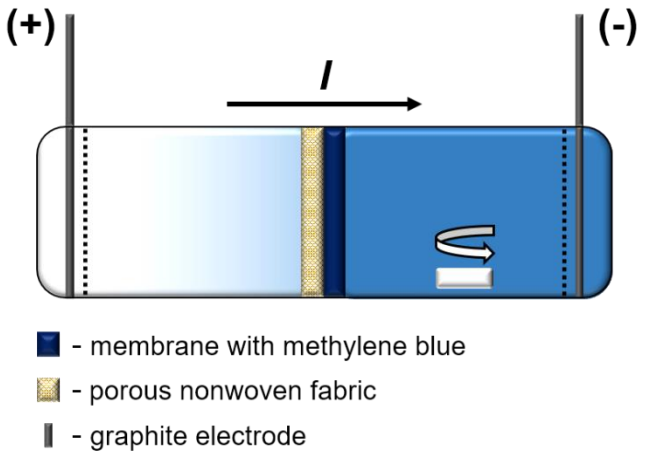

Fig. 1. Illustration of the setup for the *in vitro* iontophoresis experiment (single column image)

In the first step, membrane disk, previously equilibrated in the phosphate buffer solution (pH = 8 and I = 0.2 M), was placed between two chambers of the cell together with the piece of porous polyester spunbond nonwoven fabric. This fabric acted as a mechanical support to prevent membrane deformation possibly caused by electroosmosis phenomena during the experiment. Each chamber was filled with 1.5 ml of the concentrated MB dye (1000 ppm) and the membrane sample was allowed to absorb the dye for 24 h at ambient temperature. The interior of the cell was thoroughly rinsed with ethanol and distilled water after MB absorption to remove dye residues.

In the second step, both chambers of the cell were filled with 2 ml of the phosphate buffer solution (pH = 8 and I = 0.2 M) and cylindric graphite electrodes of 0.5 mm diameter were inserted at their ends. A stable flow of direct current with the intensity of 200 μA (or current density of about 255 μA/cm^2) was imposed between the electrodes by the external current source built in-house. The solution in the receptor chamber was continuously stirred at a speed of 500 rpm. In order to follow the kinetics of iontophoretic release, 1 ml aliquots of the receptor solution were taken with the syringe every 10 min and immediately replaced with 1 ml of fresh buffer solution. The amount of released MB in the aliquots was monitored by UV-Vis spectroscopy.

3. Results and discussion

3.1 SD, WC, and C_{cg}

Four different membrane formulations were synthesized in this work. These formulations comprised 12 or 14% PES, and 18 to 20% AA and crosslinker, by weight. The concentrations of bifunctional and trifunctional crosslinker were 10 and 5 mol%, respectively. The basic properties of the membranes are listed in **Table 1**.

Table 1. Basic properties (swelling degree (*SD*) in distilled water, water content (*WC*), carboxyl group concentration (C_{cg}), and reaction yield) with their corresponding standard deviations of membranes synthesized from different casting solutions. Legend: PES - polyethersulfone, AA - acrylic acid, MBAA - *N, N′*-Methylenebis(acrylamide), and TMPTA - trimethylolpropane ethoxylate triacrylate.

Composition of the casting solution	SD_{dw} (%)	*WC* (%)	C_{cg} (mmol/g)	Reaction yield (%)
12 wt% PES, 7 mmol/g AA, 10 mol% MBAA	161 ± 40	61 ± 6	5.20 ± 0.14	74 ± 2
14 wt% PES, 6.5 mmol/g AA, 10 mol% MBAA	151 ± 36	60 ± 6	5.13 ± 0.21	79 ± 3
12 wt% PES, 5.3 mmol/g AA, 5 mol% TMPTA	304 ± 60	75 ± 4	4.41 ± 0.01	83 ± 1
14 wt% PES, 5 mmol/g AA, 5 mol% TMPTA	265 ± 46	72 ± 4	4.87 ± 0.06	97 ± 1

One of the major differences between the membrane formulations made at equivalent PES concentration was the hydrophobic or hydrophilic nature of the crosslinker used. The hydrophobic MBAA crosslinker yields membranes with a significantly lower swelling degree and water content compared to the membranes made with the hydrophilic TMPTA crosslinker. In both cases, the presence of the PES polymeric support limits hydrogel swelling and improves the mechanical stability of the membranes. C_{cg} is slightly lower for membranes made with TMPTA than for the corresponding membranes made with MBAA. Reaction yields for the membranes calculated as the ratios of C_{cg} in the membrane and initial AA concentration have significantly higher values when TMPTA was used instead of MBAA (see **Table 1**).

The greater swelling degree of the membranes synthesized with TMPTA can be attributed to the larger size of the crosslinker molecule in comparison with MBAA, which increases the distance between neighboring crosslinks, and to the hydrophilic nature of TMPTA crosslinker. C_{cg} of the membranes synthesized with TMPTA is slightly lower despite the higher reaction yield, which mainly arises from the lower initial concentrations of AA in the casting solutions. Wet membranes synthesized with MBAA exhibited the strong

tendency to curl and roll up. These membranes had a different texture at the top (plastic-like) and bottom (gel-like) surface. On the other hand, wet membranes synthesized with TMPTA have homogeneous gel-like surface texture on both sides and are less prone to mechanical deformation.

Ion exchange capacities of our composite membranes shown in **Table 1** are generally higher than those for weakly acidic cation exchange membranes reported in the literature, i.e. 1.0 mmol/g [19], or 3.7 mmol/g [18]. Ion exchange capacity of pore-filled membranes reached 5 mmol/g at the highest mass gain, but these composite membranes were fragile due to high swelling pressures acting on the PVDF matrix [17]. A superior exchange capacity can be obtained with some weakly acidic commercial cation exchange resins and fibers, such as AMBERLITE^{TM} IRP64 (~10 mmol/g) [25] and Smopex$^{®}$-102 (6.4 mmol/g) [12], respectively. However, one advantage of the composite membrane described in this work is the possibility to control both the ion exchange capacity and kinetics by modifying the composition of the casting solution, which is hard to achieve in commercial resins and fibers.

3.2 FTIR

FTIR-ATR spectra in **Fig. 2a** reveal the asymmetric structure of wet membranes synthesized with the hydrophobic crosslinker MBAA. The top membrane side contains more PES, while the bottom side contains more PAA hydrogel, as reflected by the relative peak intensities. The spectra exhibit several absorption bands characteristic of PES: C-O stretching at 1105 cm^{-1}, symmetric SO_2 stretching at 1148 cm^{-1}, aromatic ether band of C-O-C stretching at 1238 cm^{-1}, asymmetric SO_2 stretching at 1296 and 1319 cm^{-1}, and aromatic polysulfone ring bands at 1485 and 1577 cm^{-1}. Absorption bands corresponding to the PAA hydrogel are the band indicating hydrogen bonding of carboxyl groups at 1636 cm^{-1}, C=O stretching of protonated carboxyl groups at 1705 cm^{-1}, CH_2 stretching at 2931 and 2956 cm^{-1}, and symmetric O-H stretching at 3382 cm^{-1}.

Fig. 2b shows FTIR-ATR spectra of the wet membrane synthesized with the hydrophilic crosslinker TMPTA. Top and bottom side of the membrane have almost identical spectra, which indicates a symmetric membrane structure. Compared to the spectra of the membrane synthesized with the hydrophobic crosslinker, O-H

stretching band at 3355 cm^{-1} has a higher intensity, which is consistent with the increased degree of swelling of the membrane synthesized with TMPTA.

Fig. 2c illustrates the comparison of wet and dry membrane spectra for the membranes synthesized with TMPTA. Main peaks corresponding to the PAA hydrogel disappear after the membrane was air-dried.

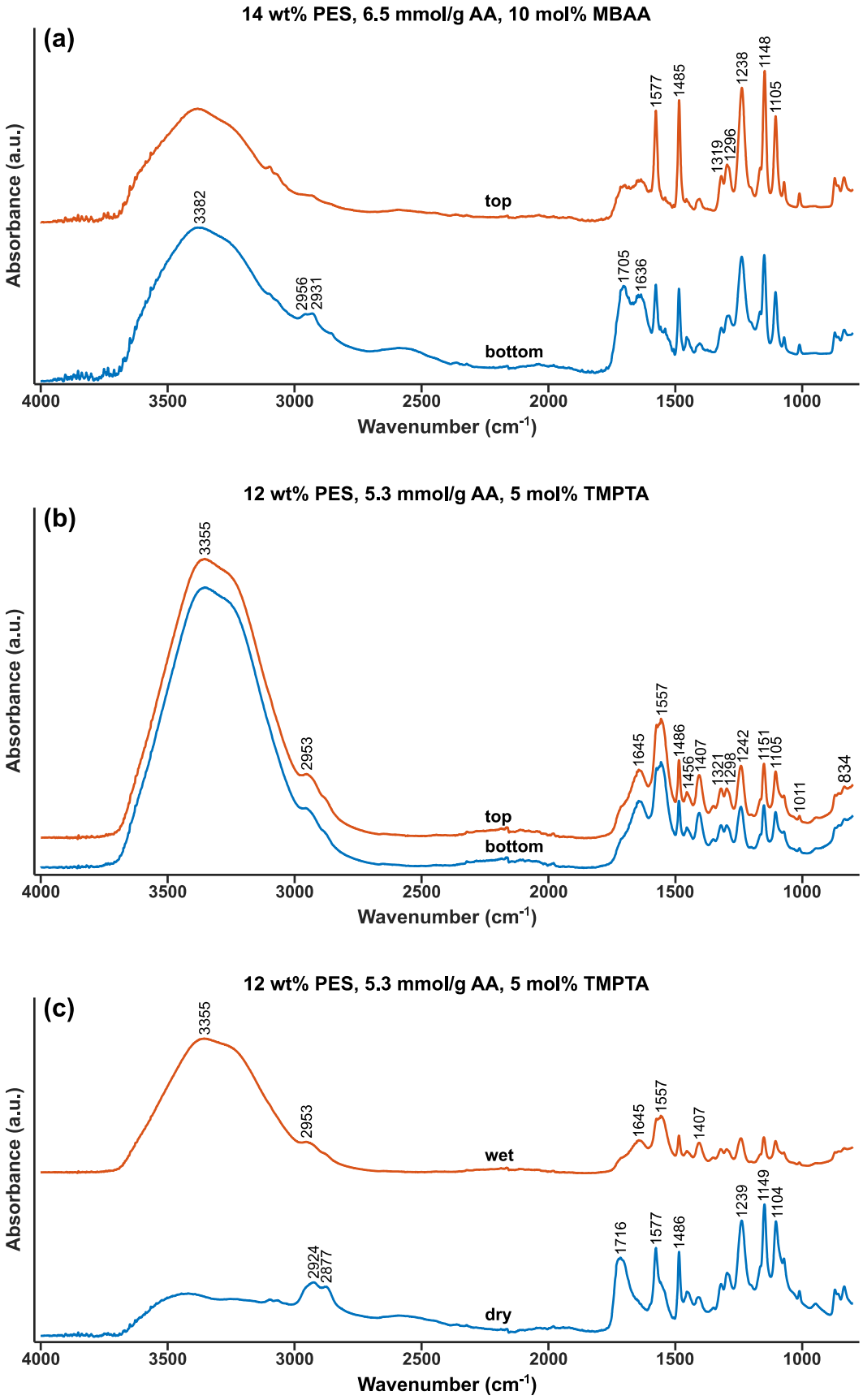

Fig. 2. FTIR-ATR spectra of the membranes synthesized from different casting solution formulations: (a) wet top and bottom surfaces of the membrane synthesized from 14 wt% PES, 6.5 mmol/g AA, 10 mol% MBAA, (b) wet top and bottom surfaces of the membrane

synthesized from 12 wt% PES, 5.3 mmol/g AA, 5 mol% TMPTA, and (c) wet and dry top surfaces of the membrane synthesized from 12 wt% PES, 5.3 mmol/g AA, 5 mol% TMPTA. Legend: PES - polyethersulfone, AA - acrylic acid, MBAA - *N*, *N*′-Methylenebis(acrylamide), and TMPTA - trimethylolpropane ethoxylate triacrylate. (1.5 column image)

New bands confirming the presence of PAA in the dry membrane become prominent in the spectrum: C=O stretching of protonated carboxyl groups at 1716 cm^{-1}, and CH_2 stretching bands at 2877 and 2924 cm^{-1}. Asymmetric structure of the membranes synthesized with MBAA which contain a PES-rich side causes mechanical instability and presumably reduces through-membrane electrical conductivity. These issues make such membranes unsuitable for handling and iontophoretic drug delivery which are some of the goals in our work. For these reasons, we continued our investigations with the more promising formulations containing TMPTA crosslinker. As both formulations with TMPTA have similar basic properties, membrane samples synthesized from the casting solution comprising 12 wt% PES, 5.3 mmol/g AA, and 5 mol% TMPTA were used as representative.

3.3 SEM

SEM images of the membrane cross-section in **Fig. 3** illustrate a symmetric membrane structure with the thickness of about 85 μm in the dry state. The microstructure is heterogeneous, comprising a porous PES matrix and spheroidal hydrogel particles with the mean diameter of 280 nm. Hydrogel particles are aggregated into small independent clusters attached to the pore walls of the PES support.

Such microstructure results from a complex interplay of phenomena which occur during membrane formation as described previously [22,26]. UV photoirradiation triggers the polymerization and crosslinking of AA and thereby an organogel is formed in the cast film. During the UV exposure, cast film becomes cloudy indicating the onset of phase separation induced by polymerization and crosslinking. Irradiated cast films formed white hydrogel-filled membranes after immersion and solidification in the water bath. The presence of water creates highly unstable thermodynamic conditions leading to the rapid completion of phase separation into the hydrophilic hydrogel-rich phase containing mainly crosslinked PAA and hydrophobic PES-rich phase surrounding the hydrogel. Polymer gels commonly exhibit nonuniform spatial distributions of polymer network concentration and crosslinking density on a local level [27].

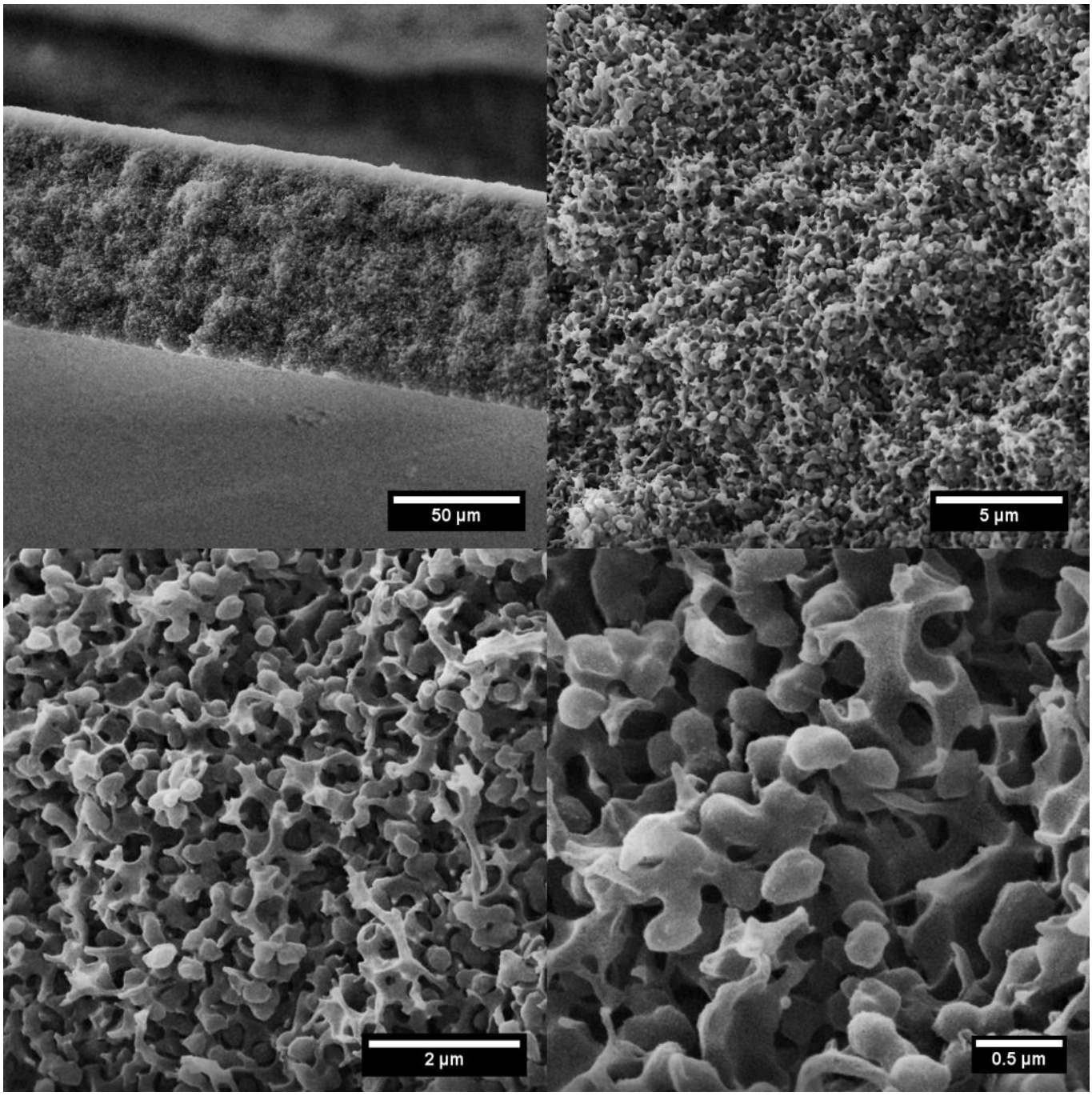

Fig. 3. SEM images of the dried membrane synthesized from the casting solution composition with 12 wt% PES, 5.3 mmol/g AA, and 5 mol% TMPTA. Legend: PES - polyethersulfone, AA - acrylic acid, and TMPTA - trimethylolpropane ethoxylate triacrylate. (full-width (2-column) image)

Similarly, UV-cured composite membranes presented in this work comprise small independent clusters of aggregated submicron hydrogel particles scattered throughout the porous PES matrix. Formation of small independent clusters of hydrogel particles can be explained by a higher rate of bi- or trifunctional crosslinker

polymerization compared to the monofunctional AA monomer, which leads to the formation of microgels after the crosslinker depletion. The hydrogel particles and aggregates remain attached to the PES support by the common polymer chains which are a result of incomplete polymer/polymer demixing in the phase separation process.

3.4 Absorption of MB

Mass of absorbed MB normalized per dry membrane mass is shown in **Fig. 4**. The amount of absorbed MB in the membrane sample after 24 h depends on the initial molar ratio $n(MB^+)/n(-COOH)$. The greater value of $n(MB^+)/n(-COOH)$ in the absorption solution corresponds to the larger driving force in the process of ion exchange and increases the loading efficiency.

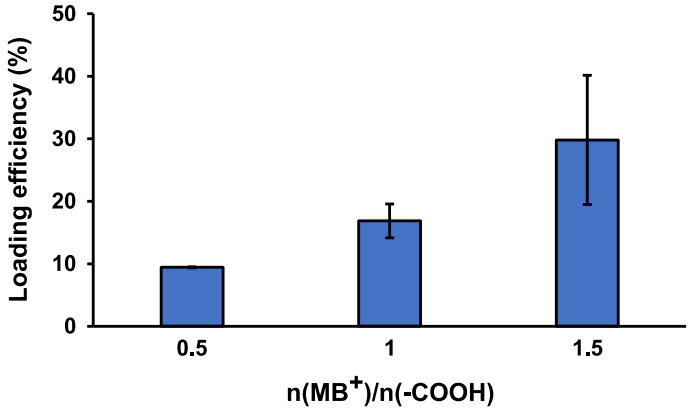

Fig. 4. Dependence of loading efficiency for MB from the initial molar ratio $n(MB^+)/n(-COOH)$ given as the mean ± standard deviation (n = 3). The maximum loading efficiency of 100% is defined as the measured ion exchange capacity for the membrane synthesized from the casting solution composition with 12 wt% PES, 5.3 mmol/g AA, and 5 mol% TMPTA. Legend: MB - methylene blue, PES - polyethersulfone, AA - acrylic acid, and TMPTA - trimethylolpropane ethoxylate triacrylate. (single column image)

Maximum loading efficiency achieved under the conditions used in the absorption experiments is slightly less than 30% of the theoretical binding capacity for MB. Higher loading efficiency could potentially be achieved with a longer absorption period or even higher initial molar ratio $n(MB^+)/n(-COOH)$. Hence, membrane samples are in the pseudo-equilibrium state after MB absorption in our experiments.

3.5 Release of MB

Relative desorption of MB Q_t/Q_e in buffer solutions is presented as a function of time in **Fig. 5.** Concentrations of MB sorbate, Q_t and Q_e, were normalized per final concentrations of MB in the solutions reached at least 48 h after the release experiments.

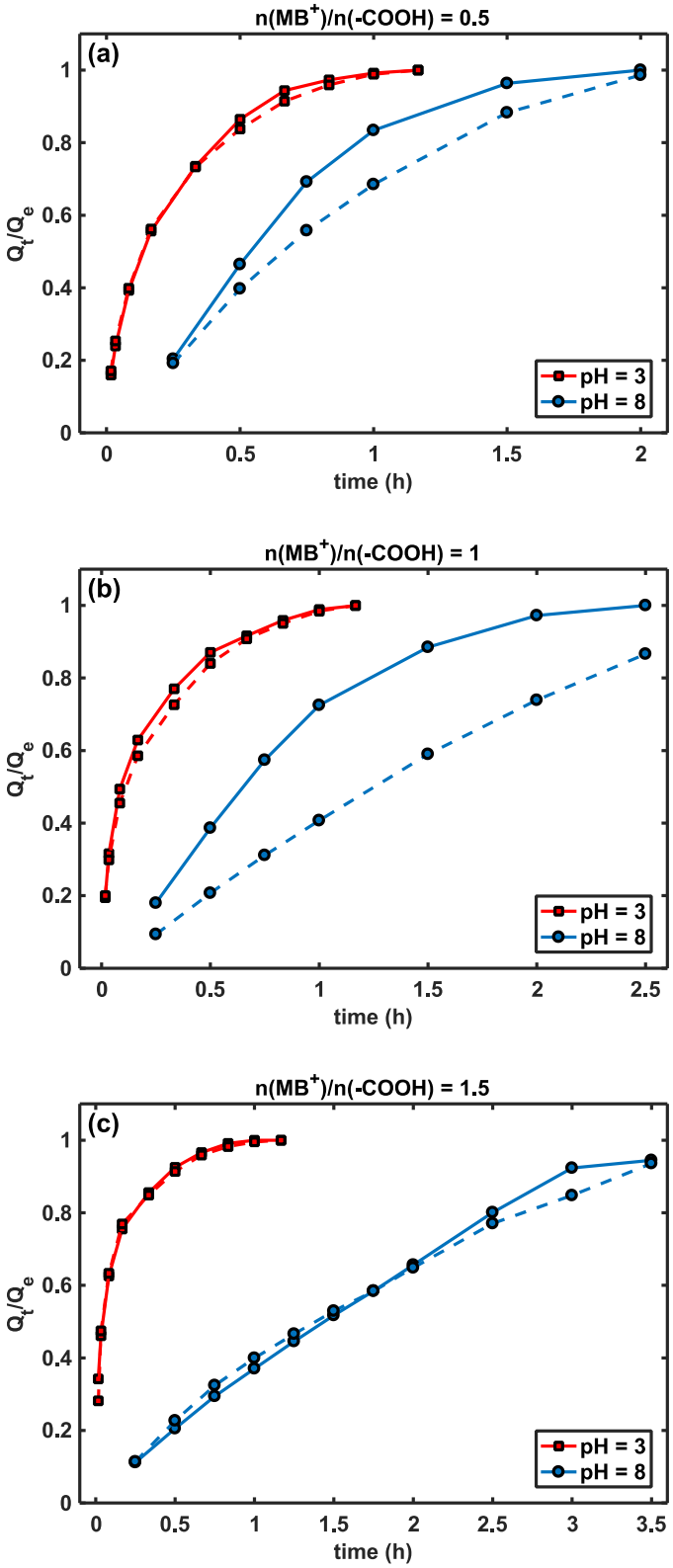

Fig. 5. *In vitro* kinetics of passive release in buffer solutions at pH = 3 and pH = 8 from membranes synthesized from the casting solution composition with 12 wt% PES, 5.3 mmol/g AA, and 5 mol% TMPTA and loaded with MB in absorption solutions with different initial molar ratios $n(MB^+)/n(-COOH)$: (a) $n(MB^+)/n(-COOH) = 0.5$, (b) $n(MB^+)/n(-COOH) = 1$, and (c) $n(MB^+)/n(-COOH) = 1.5$. Continuous and dashed lines between the markers indicate two independent measurements. Legend: MB - methylene blue, PES - polyethersulfone, AA - acrylic acid, and TMPTA - trimethylolpropane ethoxylate triacrylate. (single column image)

Individual masses of released MB per dry unit mass of the membrane can be calculated by using the known masses of the dry membrane samples and spectrophotometric calibration curves.

At pH = 3, relative desorption exhibited pseudo-Fickian behavior in all experiments. Total release period was overall independent of $n(MB^+)/n(-COOH)$ and shorter than at pH = 8.

At pH = 8, relative desorption of MB initially exhibited Fickian behavior, but the overall release kinetics was clearly non-Fickian. It is evident that the desorption from the samples loaded with MB from solutions with $n(MB^+)/n(-COOH) = 1.5$ was governed by the two-stage kinetics comprising the slower diffusion-controlled release for small times and faster release after the initial period. Total release period increased in proportion with $n(MB^+)/n(-COOH)$.

Comparisons of the masses of MB released per unit mass of the dry membrane in buffer solutions and 96% ethanol give the approximate ratio of MB amount bound by electrostatic and hydrophobic forces, respectively (see data in **Table S1** in the **Supplementary Information**). At least 91% of MB in the membrane samples was electrostatically bound. On average, up to 36% smaller amount of MB was released in the buffer solution at pH = 3 compared to the amount released in the buffer solution at pH = 8 after the same MB absorption protocol. Incomplete release at pH = 3 is presumably a consequence of rapid membrane deswelling which tends to trap a part of MB in collapsed microgels.

We made an attempt to evaluate the release kinetics of MB by fitting experimental data to the Korsmeyer-Peppas equation [28] which is widely used to investigate solute release from polymer matrices:

$$\frac{M_t}{M_\infty} = kt^n \tag{4}$$

where M_t/M_∞ is the fractional solute release, k is the characteristic kinetic constant of the polymer/solute system, and n is the diffusional exponent characterizing the release mechanism. To obtain a more adequate regression model, Eq. **(4)** was linearized using the log-log transformation:

$$\log\left(\frac{M_t}{M_\infty}\right) = \log k + n \log t \tag{5}$$

This approach was also adopted by Osváth et al. [29] when analyzing organic-inorganic hybrid composite thermoresponsive hydrogels. Parameters obtained by linear regression are provided in **Table 2**. Fits of the release kinetics for small times obtained by using the linearized form of Korsmeyer-Peppas equation are given in **Fig. S1**.

Table 2. Kinetic constants (k), diffusional exponents (n), with their associated standard deviations (sd) and coefficients of determination (R^2) calculated based on the methylene blue (MB) desorption experiments conducted under different experimental conditions of pH and the initial molar ratio ($n(MB^+)/n(-COOH)$).

pH	$n(MB^+)/n(-COOH)$	$k \pm sd$ (h^{-n})	$n \pm sd$	R^2
3	0.5	1.457 ± 0.045	0.528 ± 0.019	0.999
	1	1.866 ± 0.338	0.541 ± 0.047	0.993
	1.5	1.931 ± 0.471	0.433 ± 0.085	0.968
8	0.5	0.803 ± 0.126	0.981 ± 0.078	0.991
	1	0.573 ± 0.253	1.004 ± 0.016	0.996
	1.5	0.376 ± 0.011	0.834 ± 0.019	0.996

Despite the statistically sound regression results, this empirical model is not completely physically plausible. Eq. **(4)** provides adequate description up to 60% of fractional release only for systems where the release occurs in perfect sink conditions [30]. These authors clearly state that in the more realistic situation of variable boundary conditions, empirical Eq. **(4)** cannot be used to correctly describe the release behavior.

The release of MB from our composite membranes is quite complex and involves several processes. Diffusion of buffer cations into the membrane initiates ion exchange reaction and just after its completion MB cations can diffuse through the membrane and finally get released to the solution. Release to the bulk solution by diffusion additionally requires that MB cations overcome the boundary layer resistance. Each of this processes requires finite time which cannot be neglected, and thus the perfect sink approximation is not applicable. For this reason,

we turn to the analytical model based on diffusion from thin films [31] supplemented with the empirical Weber-Morris model [32].

Kinetics of MB desorption from the composite hydrogel membrane can be approximately described as a diffusion-controlled process. Such description is adequate since the diffusive transport of MB through the hydrogel phase is a significantly slower process compared to the electrostatic interactions involved in MB desorption. An intramembrane diffusion model (IMD) can be obtained by applying the formalism of the intraparticle diffusion model to the plane sheet particle geometry [33]. The basic equation of the model governing the desorption process can then be written as:

$$\frac{\partial C}{\partial t} = \frac{D}{\tau}\frac{\partial^2 C}{\partial x^2} - \frac{\rho}{\varepsilon_p}\frac{\partial q}{\partial t} \tag{6}$$

with the following boundary condition:

$$\left(\frac{\partial C}{\partial x}\right)\Big|_{x=0} = 0 \tag{7}$$

and initial conditions at $t = 0$:

$$\begin{gathered} C(-l < x < l) = C_0 \\ C(x = \pm l) = 0 \end{gathered} \tag{8}$$

In the basic equation, C and q are the local sorbate concentrations in the membrane hydrogel phase and the surrounding solution, which are related by the equilibrium relationship, D is the molecular diffusion coefficient in the hydrogel phase, ρ is membrane density, ε_p is membrane porosity equal to the fractional hydrogel volume, and τ is the so-called tortuosity factor, which for interconnected porous structures equals to the reciprocal of the square root of porosity [34]. In the initial conditions, C_0 is the sorbate concentration within the membrane at $t = 0$ which is considered to be uniform, and l is half of the membrane thickness. The problem geometry is taken to be symmetric about the central plane. When the assumptions of constant sorbate concentration at the membrane/solution interface and applicability of Henry's law hold, analytical solution yielding the relative desorption q_t/q_e can be found as:

$$\frac{q_t}{q_e} = 1 - \frac{8}{\pi^2}\sum_{n=0}^{\infty}\frac{1}{(2n+1)^2}exp\left(-\frac{D_a\pi^2(2n+1)^2}{4l^2}t\right) \quad (9)$$

where D_a is the apparent diffusion coefficient, while q_t and q_e denote the sorbate concentration in the solution at time t and in equilibrium at the end of the desorption process, respectively.

Relation of D_a to D and composite hydrogel membrane parameters is given by:

$$D_a = \frac{D}{\tau\left(1+\rho K_H/\varepsilon_p\right)} \quad (10)$$

where K_H represents Henry's constant.

The analytical solution in Eq. **(9)** is the same as the solution to the problem of non-steady state diffusion in a plane sheet where the diffusing component is initially uniformly distributed and with equal surface concentrations [31]. Hence, Eq. **(9)** can be written in the following form for small times:

$$\frac{q_t}{q_e} = 2\left(\frac{D_a t}{l^2}\right)^{0.5}\left(\pi^{-0.5} + 2\sum_{n=1}^{\infty}(-1)^n ierfc\left(\frac{nl}{(D_a t)^{0.5}}\right)\right) \quad (11)$$

When the argument of an *ierfc* function in Eq. **(11)** takes large values, the value of *ierfc* function approaches zero. Such result suggests, that for small times relative desorption should be closely proportional to $t^{0.5}$.

If the conditions of the perfect sink are relaxed, desorption of MB can be described by empirical Weber-Morris equation [32]:

$$\frac{q_t}{q_e} = at^{0.5} + b \quad (12)$$

where a is interpreted as the rate parameter and b as the intercept proportional to the boundary layer thickness determining the resistance to mass transfer. For short times, Eqs. **(11)** and **(12)** can be combined to yield:

$$\frac{q_t}{q_e} = 2\left(\frac{D_a t}{\pi l^2}\right)^{0.5} + b \quad (13)$$

Based on a separate analysis of the maximum time for which Eq. **(13)** has a good accuracy for desorption (q_t/q_e < 2/3) [31], we determined the number of initial points used for the linear fit independently for each series of MB release experiments. We later used the slope of the fitted lines to calculate D_a. Parameter l in the expression

391 for the slope is half of the wet membrane thickness calculated based on the wet mass of the membrane sample,
392 average *SD*, measured area, and estimated mean density.
393 The release kinetics for MB is strongly dependent on the initial molar ratio $n(MB^+)/n(\text{-COOH})$ and pH of the
394 buffer solution. As shown in section **3.4 Absorption of MB**, higher $n(MB^+)/n(\text{-COOH})$ improves the loading
395 efficiency, which consequently leads to the stabilizing electrostatic interactions and reduced membrane
396 swelling. pH-sensitive hydrogel phase also survives swelling transients in the buffer solution during desorption
397 which affects the MB release kinetics. Such pH-dependent behavior of the hydrogel is largely defined by the
398 state of charge in carboxyl groups of PAA which are negatively charged at pH = 8 and mainly protonated at pH
399 = 3. The influence of $n(MB^+)/n(\text{-COOH})$ and pH on swelling transients can be roughly estimated from the mass
400 swelling degrees obtained for pure buffer solutions (see **Fig. 6**) and solutions for MB loading with different
401 $n(MB^+)/n(\text{-COOH})$ after 24 h of absorption (see **Fig. 7**).
402 As can be concluded from the IMD, membrane thickness is also an important parameter determining the release
403 kinetics. Variations in casting speed can significantly affect the thickness of individual membrane samples,
404 while the irregularities at the membrane surface and swelling transients can cause significant thickness
405 variations locally. Effects of thickness should be prominent at pH = 8 when membrane samples continuously
406 swell during MB release while being much less significant at pH = 3 due to strong and rapid deswelling. This is
407 corroborated by our release experiments where much larger deviations in the release kinetics occur at pH = 8
408 (see **Fig. 5**). Such deviations can be completely explained by the difference in average membrane thickness
409 between samples of up to 25% (see **Fig. 5b**) using the IMD (data not shown).

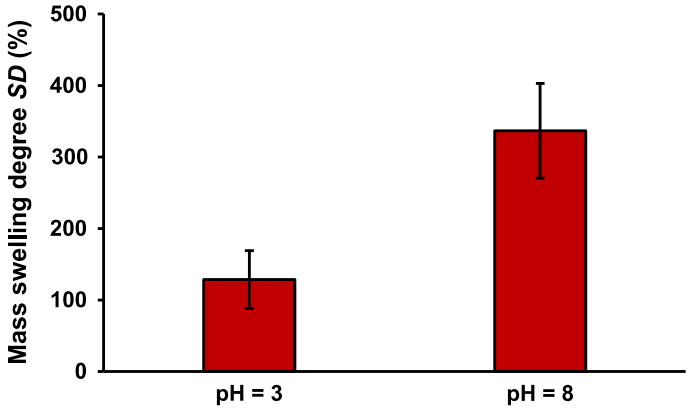

410

Fig. 6. Mass swelling degree (*SD*) in the buffer solutions for the membrane synthesized from the casting solution composition with 12 wt% PES, 5.3 mmol/g AA, and 5 mol% TMPTA given as the mean ± standard deviation (n = 3). Legend: PES - polyethersulfone, AA - acrylic acid, and TMPTA - trimethylolpropane ethoxylate triacrylate. (single column image)

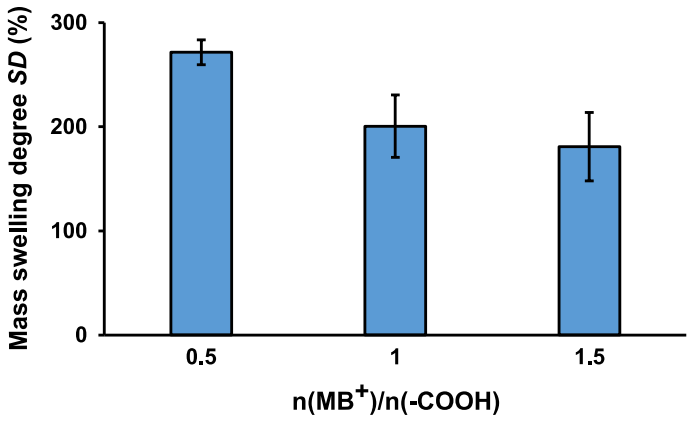

Fig. 7. Mass swelling degree (*SD*) in the MB absorption solutions for the membrane synthesized from the casting solution composition with 12 wt% PES, 5.3 mmol/g AA, and 5 mol% TMPTA given as the mean ± standard deviation (n = 3). Legend: MB - methylene blue, PES - polyethersulfone, AA - acrylic acid, and TMPTA - trimethylolpropane ethoxylate triacrylate. (single column image)

Two-stage desorption kinetics from the membrane samples with highest MB loading at pH = 8 can be explained by hydrogel relaxation occurring after the initial release phase. Densely packed electrostatically bound MB cations limit the mobility of hydrogel chains thereby reducing the swelling and the apparent diffusion coefficient. Relaxation effect is not significant at pH = 3 for the samples with a similar amount of loaded MB, due to the dominant deswelling caused by carboxyl group protonation.

In all release experiments, a linear relationship between the relative desorption Q_t/Q_e and $t^{0.5}$ was observed during the initial period (see **Fig. S2** in the **Supplementary Information**).

Table 3. Apparent diffusion coefficients (D_a) and intercepts of the empirical Weber-Morris equation (*b*) with their associated standard deviations (*sd*), and coefficients of determination (R^2) calculated based on the methylene blue (MB) desorption experiments conducted under different experimental conditions of pH and initial molar ratio (n(MB^+)/n(-COOH)).

pH	n(MB^+)/n(-COOH)	$D_a \pm sd$ ($\times 10^{-12}$ m^2/s)	$b \pm sd$	R^2
3	0.5	1.852 ± 0.049	-0.013 ± 0.011	1.000
	1	2.764 ± 0.607	-0.017 ± 0.026	0.995
	1.5	3.492 ± 0.906	0.085 ± 0.060	0.966
8	0.5	1.870 ± 0.668	-0.368 ± 0.094	0.999

1	1.003 ± 0.607	-0.333 ± 0.061	0.996
1.5	0.384 ± 0.016	-0.196 ± 0.022	0.996

As **Table 3** shows, coefficients of determination were in most cases larger than 0.99, and in statistical terms, there was practically no difference between coefficients of determination for Korsmeyer-Peppas model (see **Table 2**) and the model which combined the analytical solution and Weber-Morris empirical model (see **Table 3**). Intercepts of the linear fits describing desorption kinetics can be explained by the differences in the boundary layer resistance. Negative intercepts of the fits describing the kinetics at pH = 8 can be interpreted as the measure of the boundary layer resistance for the desorption process [35]. The greater density of uncompensated negative charges at the membrane/solution interface for membranes less loaded with MB ions, causes the increase in the boundary layer resistance, as shown by the value of intercepts in **Table 3**. Intercepts of the linear fits describing desorption kinetics at pH = 3 are shifted towards more positive values, which indicates the existence of an additional effect counteracting the boundary layer resistance to the release of MB. This effect can be attributed to the initial convective flow arising at the membrane/solution interface. We have visually confirmed the initial burst release of MB lasting several seconds in all release experiments conducted at pH = 3. Protonation of carboxyl groups via ion exchange of MB cations with highly mobile hydronium ions boosts the release of MB through the formation of a repulsive electrostatic force and rapid membrane deswelling. The intensity of the repulsive force is greater for higher membrane loadings with MB cations due to the increased amount of charge.

Apparent diffusion coefficient for the release at pH = 3 increases with the initial MB loading and is generally greater than for the release at pH = 8 (see **Table 3**). This trend can be attributed to the electrostatically-assisted release where the repulsive force is proportional to the total charge accumulated by MB cations. Some amount of water containing dissolved MB presumably stays entrapped within the porous polymer base outside of the hydrogel phase after membrane deswelling. The rate-limiting diffusive transport of MB is then facilitated and potentially faster than within the hydrogel phase.

The effect of initial MB loading on the release kinetics and apparent diffusion coefficient of MB at pH = 8 can also be analyzed from the perspective of average membrane pore size. Pore size can be estimated from the

calculation of PAA gel correlation length according to the previous research of Hu and Dickson on similar membrane structures [36]. Using the correlation length approach, we obtain the average effective pore diameter of around 2.3 nm without loaded MB. With the increase in MB loading, the pore diameter is reduced, and at the highest initial MB loading, the average pore diameter is estimated to be 1.7 nm. Specific details about the calculation are provided in the **Supplementary Information** section **Estimation of membrane pore size using the gel correlation length model**. Shrinking of the pores in the matrix with the increase of MB content can be attributed to the more probable electrostatic ion pairing between the positively charged MB ions and negatively charged PAA chains. Size of the MB molecule (0.591 nm x 1.382 nm [37]) is comparable to the average pore diameter. Hence, the changes in pore size induced by MB loading are expected to strongly affect the apparent diffusion coefficient and lead to the accelerated release of MB in the later stages of desorption. Distinct stages of accelerated release should be observed more easily for higher initial MB loadings which is corroborated by our experiments.

Apparent diffusion coefficients of MB in our composite hydrogel membrane are about one order of magnitude smaller than the diffusion coefficients reported in the literature for MB diffusion in poly(ethylene glycol) diacrylate hydrogels [38]. Such result is to be expected due to the presence of porous PES matrix surrounding hydrogel, which additionally limits the diffusive transport of MB.

3.6 In vitro iontophoresis

We conducted an *in vitro* iontophoresis experiment to demonstrate the potential of our composite membranes to serve as reservoirs for cationic formulations in iontophoresis. As shown in **Fig. 8**, iontophoretic release kinetics for MB is linear. Positive intercept can be attributed to the amount of MB released into the buffer solution during the setup of the experiment before the flow of electric current was established.

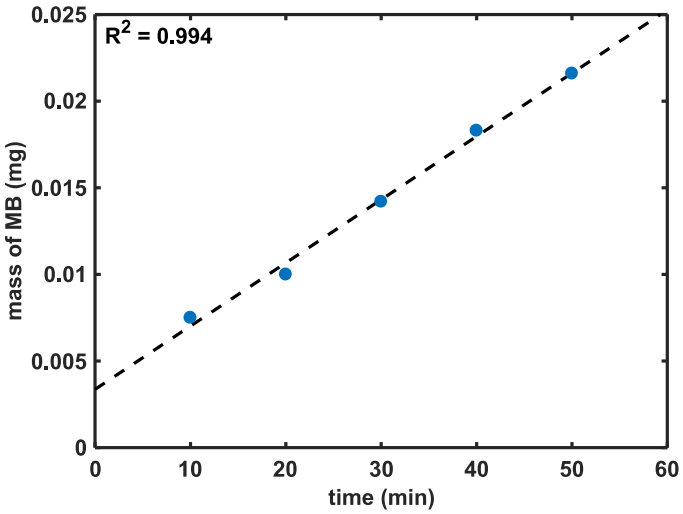

Fig. 8. Kinetics of methylene blue (MB) release recorded in the *in vitro* iontophoretic release demonstration experiment. (single column image)

At the beginning of the experiment, wet membrane contains the absorbed cations of MB and the buffer cations. Due to the permselectivity of the membrane, current flow through the membrane mainly occurs via the transport of cations which are transferred towards the receptor solution. The electric current carried by MB cations calculated from the slope of the fitted line is about 2 μA which amounts to around 1% of the total current. Such result is expected since the competing cations of the buffer solution have significantly smaller mass and greater ionic mobilities. The linear release kinetics observed during this experiment indicates that the application of our composite membranes for iontophoretic drug delivery deserves further investigation.

4. Conclusions

We have presented the innovative design and synthesis of composite hydrogel membranes comprising the PES porous base and PAA hydrogel. The key parameter determining final membrane properties was the nature of the crosslinker used in the casting solution. Our membranes have the ion exchange capacity comparable with the pharmaceutical grade ion exchange resins, moderate *SD* and mechanical stability required to serve as cationic drug reservoirs without additional components. Modifications of the casting solution composition can be utilized to adjust the ion exchange capacity, and (combined with the drug loading conditions) to define the

passive diffusion-controlled drug release kinetics. We have also tested the potential for the use of composite hydrogel membranes as reservoirs in iontophoretic delivery and obtained linear release kinetics in an *in vitro* demonstration experiment. Fabricated composite hydrogel membranes show great promise for use in the treatment of chronic wounds and transdermal drug delivery. The focus of our future research will be on detailed investigations of composite hydrogel membranes as drug matrices for iontophoretic delivery.

Acknowledgments

This work was supported by the Ministry of Education, Science and Technological Development of the Republic of Serbia, under the grant TR32008. We would like to acknowledge Assistant Professor Dr. Đorđe Veljović, from the Department of Inorganic Chemical Technology, Faculty of Technology and Metallurgy, University of Belgrade, Serbia, for acquiring SEM images of membrane samples.

Declarations of interest: none.

Appendix A. Supplementary data

Supplementary data related to this article can be found at (link)

Note: Supplementary information. The graphical representations of release kinetics fitting by the Korsmeyer-Peppas and Weber-Morris equations are provided. Masses of released methylene blue under different experimental conditions are given in a separate table. Estimation of membrane pore size at pH = 8 was performed using the gel correlation length model. (PDF)

References

[1] N.A. Peppas, P. Bures, W. Leobandung, H. Ichikawa, Hydrogels in pharmaceutical formulations, Eur. J. Pharm. Biopharm. 50 (2000) 27–46. doi:10.1016/S0939-6411(00)00090-4.

[2] E. Caló, V. V. Khutoryanskiy, Biomedical applications of hydrogels: A review of patents and

commercial products, Eur. Polym. J. 65 (2015) 252–267. doi:10.1016/j.eurpolymj.2014.11.024.

[3] T.R. Hoare, D.S. Kohane, Hydrogels in drug delivery: Progress and challenges, Polymer (Guildf). 49 (2008) 1993–2007. doi:10.1016/j.polymer.2008.01.027.

[4] B. Iván, J.P. Kennedy, P.W. Mackey, Amphiphilic Networks, United States Patent 5,073,381, 1991.

[5] P.I. Lee, C.-J. Kim, Probing the mechanisms of drug release from hydrogels, J. Control. Release. 16 (1991) 229–236. doi:10.1016/0168-3659(91)90046-G.

[6] S. Hahn, Polyurethane hydrogel compositions for iontophoretic drug delivery., EP0524718A1, 1993.

[7] M. Vuorio, J.A. Manzanares, L. Murtomäki, J. Hirvonen, T. Kankkunen, K. Kontturi, Ion-exchange fibers and drugs: A transient study, J. Control. Release. 91 (2003) 439–448. doi:10.1016/S0168-3659(03)00270-0.

[8] J.V. Stamenković, P.I. Premović, S.V. Mentus, Electrical conductivity of poly(acrylic acid) gels, J. Serbian Chem. Soc. 62 (1997) 945–950.

[9] P. Singh, H.I. Maibach, Iontophoresis in drug delivery: basic principles and applications., Crit. Rev. Ther. Drug Carrier Syst. 11 (1994) 161–213. http://www.ncbi.nlm.nih.gov/pubmed/7600587 (accessed January 2, 2018).

[10] D.F. Stamatialis, Drug Delivery Through Skin: Overcoming the Ultimate Biological Membrane, in: K.-V. Peinemann, S.P. Nunes (Eds.), Membr. Life Sci., WILEY-VCH Verlag GmbH & Co, Weinheim, 2008: pp. 198–204.

[11] T. Jaskari, M. Vuorio, K. Kontturi, A. Urtti, J.A. Manzanares, J. Hirvonen, Controlled transdermal iontophoresis by ion-exchange fiber., J. Control. Release. 67 (2000) 179–90. doi:10.1016/S0168-3659(00)00204-2.

[12] K. Malinovskaja, T. Laaksonen, K. Kontturi, J. Hirvonen, Ion-exchange and iontophoresis-controlled delivery of apomorphine., Eur. J. Pharm. Biopharm. 83 (2013) 477–84. doi:10.1016/j.ejpb.2012.11.014.

[13] K. Malinovskaja, T. Laaksonen, J. Hirvonen, Controlled transdermal delivery of leuprorelin by pulsed iontophoresis and ion-exchange fiber., Eur. J. Pharm. Biopharm. 88 (2014) 594–601.

doi:10.1016/j.ejpb.2014.08.010.

[14] Y. Gao, J. Yuan, H. Liu, Y. Yang, Y. Hou, S. Li, Tramadol loading, release and iontophoretic characteristics of ion-exchange fiber, Int. J. Pharm. 465 (2014) 102–111. doi:10.1016/j.ijpharm.2014.02.017.

[15] P. D. Vispute, M.P. Wagh, N.N. Inamdar, Comparative Evaluation Of Ion Exchange Resins And Fibers In Iontophoretic Transdermal Delivery Of Sumatriptan Succinate, Adv. Mater. Lett. 7 (2016) 754–759. doi:10.5185/amlett.2016.6158.

[16] Q. Yang, N. Adrus, F. Tomicki, M. Ulbricht, Composites of functional polymeric hydrogels and porous membranes, J. Mater. Chem. 21 (2011) 2783–2811. doi:10.1039/C0JM02234A.

[17] K. Hu, J.M. Dickson, Development and characterization of poly(vinylidene fluoride)-poly(acrylic acid) pore-filled pH-sensitive membranes, J. Memb. Sci. 301 (2007) 19–28. doi:10.1016/j.memsci.2007.05.031.

[18] Q. Wei, J. Li, B. Qian, B. Fang, C. Zhao, Preparation, characterization and application of functional polyethersulfone membranes blended with poly (acrylic acid) gels, J. Memb. Sci. 337 (2009) 266–273. doi:10.1016/j.memsci.2009.03.055.

[19] C.O. M'Bareck, Q.T. Nguyen, S. Alexandre, I. Zimmerlin, Fabrication of ion-exchange ultrafiltration membranes for water treatment. I. Semi-interpenetrating polymer networks of polysulfone and poly(acrylic acid), J. Memb. Sci. 278 (2006) 10–18. doi:10.1016/j.memsci.2005.10.058.

[20] C. Sun, H. Ji, H. Qin, S. Nie, W. Zhao, C. Zhao, A facile approach toward multifunctional polyethersulfone membranes via in situ cross-linked copolymerization, J. Biomater. Sci. Polym. Ed. 26 (2015) 1013–1034. doi:10.1080/09205063.2015.1071929.

[21] P. Radovanovic, M. Kellner, J. Matovic, R. Liska, T. Koch, Asymmetric membranes with interpenetrating proton-conducting morphology made by a combination of immersion precipitation and photopolymerization, J. Memb. Sci. 401–402 (2012) 254–261. doi:10.1016/j.memsci.2012.02.012.

[22] A. Stajčić, A. Nastasović, J. Stajić-Trošić, J. Marković, A. Onjia, F. Radovanović, Novel membrane-

563 supported hydrogel for removal of heavy metals, J. Environ. Chem. Eng. 3 (2015) 453–461.
564 doi:10.1016/j.jece.2015.01.005.
565 [23] K. Edwards, New Twist on an Old Favorite: Gentian Violet and Methylene Blue Antibacterial Foams,
566 Adv. Wound Care. 5 (2016) 11–18. doi:10.1089/wound.2014.0593.
567 [24] K.Y. Woo, J. Heil, A prospective evaluation of methylene blue and gentian violet dressing for
568 management of chronic wounds with local infection, Int. Wound J. 14 (2017) 1029–1035.
569 doi:10.1111/iwj.12753.
570 [25] AMBERLITE™ IRP64 Pharmaceutical Grade Cation Exchange Resin (Polacrilex Resin), Tech. Data
571 Sheet. (2006).
572 https://www.dow.com/assets/attachments/business/process_chemicals/amberlite_and_duolite_pharmaceu
573 tical_grade_resins/amberlite_irp64/tds/amberlite_irp64.pdf.
574 [26] T. Tomković, F. Radovanović, A. Nastasović, D. Vasiljević-Radović, J. Marković, B. Grgur, A. Onjia,
575 Solid phase extraction membranes with submicron multifunctional adsorbent particles, Eur. Polym. J. 63
576 (2015) 90–100. doi:10.1016/j.eurpolymj.2014.12.015.
577 [27] E.S. Matsuo, M. Orkisz, S.T. Sun, Y. Li, T. Tanaka, Origin of Structural Inhomogeneities in Polymer
578 Gels, Macromolecules. 27 (1994) 6791–6796. doi:10.1021/ma00101a018.
579 [28] R.W. Korsmeyer, R. Gurny, E. Doelker, P. Buri, N.A. Peppas, Mechanisms of solute release from porous
580 hydrophilic polymers, Int. J. Pharm. 15 (1983) 25–35. doi:10.1016/0378-5173(83)90064-9.
581 [29] Z. Osváth, T. Tóth, B. Iván, Sustained Drug Release by Thermoresponsive Sol–Gel Hybrid Hydrogels of
582 Poly(N-Isopropylacrylamide-co-3-(Trimethoxysilyl)Propyl Methacrylate) Copolymers, Macromol. Rapid
583 Commun. 38 (2017) 28–31. doi:10.1002/marc.201600724.
584 [30] P.L. Ritger, N.A. Peppas, A simple equation for description of solute release I. Fickian and non-fickian
585 release from non-swellable devices in the form of slabs, spheres, cylinders or discs, J. Control. Release. 5
586 (1987) 23–36. doi:10.1016/0168-3659(87)90034-4.
587 [31] J. Crank, The Mathematics of Diffusion, 2nd ed., Oxford University Press, London, 1975.

doi:10.1016/0306-4549(77)90072-X.

[32] W.J. Weber, J.C. Morris, Advances in water pollution research: removal of biologically resistant pollutant from waste water by adsorption, Proc. Int. Conf. Water Pollut. Symp. 2 (1962) 231–266.

[33] W. Plazinski, W. Rudzinski, A novel two-resistance model for description of the adsorption kinetics onto porous particles, Langmuir. 26 (2010) 802–808. doi:10.1021/la902211c.

[34] L. Pisani, Simple Expression for the Tortuosity of Porous Media, Transp. Porous Media. 88 (2011) 193–203. doi:10.1007/s11242-011-9734-9.

[35] G. McKay, M.S. Otterburn, A.G. Sweeney, The removal of colour from effluent using various adsorbents-III. Silica: Rate processes, Water Res. 14 (1980) 15–20. doi:10.1016/0043-1354(80)90037-8.

[36] K. Hu, J.M. Dickson, Modelling of the pore structure variation with pH for pore-filled pH-sensitive poly(vinylidene fluoride)-poly(acrylic acid) membranes, J. Memb. Sci. 321 (2008) 162–171. doi:10.1016/j.memsci.2008.04.046.

[37] J. de S. Macedo, N.B. da Costa Júnior, L.E. Almeida, E.F. da S. Vieira, A.R. Cestari, I. de F. Gimenez, N.L. Villarreal Carreño, L.S. Barreto, Kinetic and calorimetric study of the adsorption of dyes on mesoporous activated carbon prepared from coconut coir dust, J. Colloid Interface Sci. 298 (2006) 515–522. doi:10.1016/j.jcis.2006.01.021.

[38] S.M. Evans, A.L. Litzenberger, A.E. Ellenberger, J.E. Maneval, E.L. Jablonski, B.M. Vogel, A microfluidic method to measure small molecule diffusion in hydrogels, Mater. Sci. Eng. C. 35 (2014) 322–334. doi:10.1016/j.msec.2013.10.035.